

HUBBLE SPACE TELESCOPE PROPER MOTIONS OF INDIVIDUAL STARS IN STELLAR STREAMS: ORPHAN, SAGITTARIUS, LETHE, AND THE NEW “PARALLEL” STREAM

SANGMO TONY SOHN^{1,2}, ROELAND P. VAN DER MAREL², NITYA KALLIVAYALIL³, STEVEN R. MAJEWSKI³, GURTINA BESLA⁴,
JEFFREY L. CARLIN⁵, DAVID R. LAW², MICHAEL H. SIEGEL⁶, AND JAY ANDERSON²

Draft version October 26, 2018

ABSTRACT

We present a multi-epoch *Hubble Space Telescope* (*HST*) study of stellar proper motions (PMs) for four fields along the Orphan Stream. We determine absolute PMs of several individual stars per target field using established techniques that utilize distant background galaxies to define a stationary reference frame. Five Orphan Stream stars are identified in one of the four fields based on combined color-magnitude and PM information. The average PM is consistent with the existing model of the Orphan stream by Newberg et al. In addition to the Orphan stream stars, we detect stars that likely belong to other stellar streams. To identify which stellar streams these stars belong to, we examine the 2-d bulk motion of each group of stars on the sky by subtracting the PM contribution of the solar motion (which is a function of position on the sky and distance) from the observed PMs, and comparing the vector of net motion with the spatial extent of known stellar streams. By doing this, we identify candidate stars in the Sagittarius and Lethe streams, and a newly-found stellar stream at a distance of ~ 17 kpc, which we tentatively name the “Parallel stream”. Together with our Sagittarius stream study (Sohn et al., 2015, *ApJ*, 803, 56), this work demonstrates that even in the *Gaia* era, *HST* will continue to be advantageous in measuring PMs of old stellar populations on a star-by-star basis, especially for distances beyond ~ 10 kpc.

Keywords: astrometry — Galaxy: halo — Galaxy: kinematics and dynamics — proper motions

1. INTRODUCTION

Stellar streams in the Milky Way (MW) halo are direct evidence of the hierarchical nature of cold dark matter-based structure formation. They prove that our Galaxy has grown, at least in part, via the tidal disruption of dwarf galaxies and globular clusters. Discovering and characterizing tidal streams is therefore a critical test for structure formation models. On global scales, streams are powerful probes of radial profile and shape of the MW’s dark matter halo (e.g., Johnston et al. 1999; Peñarrubia et al. 2012). Because they are kinematically cold, streams are also emerging as useful tools for constraining small-scale dark matter structures: direct impacts from subhalos may dynamically heat a stream and create gaps in surface density along the debris (Johnston et al. 2002; Yoon et al. 2011; Carlberg 2012a; Carlberg et al. 2012b; Erkal & Belokurov 2015a,b; Bovy 2016).

The structure of a tidal stream dictates the regimes over which it is sensitive as a dynamical probe. A long stream such as the Sagittarius (Sgr) Stream has been mapped a full 360° on the sky and thus allows sensitivity to the global potential, but might have complicated dynamics because it is influenced by a comparatively large progenitor. By contrast, thin streams, such as those belonging to globular clusters like

Pal 5, are sensitive to small-scale lumpiness, but might suffer from limitations in their phase-space coverage and hence from degeneracies in fitting different orbital parameters to a limited set of observables (e.g., Koposov et al. 2010). In general, the parameter space involved in modeling these interactions is large, and prominently lacking are proper motions (PMs) as a function of position along a stream.

Currently, only a few PM datasets exist for streams, including patches of the Sgr Stream (Carlin et al. 2012; Koposov et al. 2014; Sohn et al. 2015), and for the GD-1 Stream (Koposov et al. 2010), which is unfortunately very close in and probes the Galactic disk rather than the halo. The Sgr Stream is the brightest and most prominent stellar stream in the MW and probes the halo. As a result it has been the topic of intense data-collection and modeling efforts. In the past, no one model had been capable of simultaneously reproducing both the angular position and the distances/radial velocities of tidal debris in the Sgr leading arm in a static axisymmetric MW dark halo. Law et al. (2009) showed that the data can be reconciled by adopting a triaxial halo for the MW. The best fit halo model is then near oblate but with its symmetry axis perpendicular to that of the MW disk (Law & Majewski 2010; Deg & Widrow 2013). Although this work represents one of the most sophisticated data-model comparisons to date, its conclusions are quite surprising and has been the topic of intense debate (Debattista et al. 2013). Moreover, in recent works uncovering new Sgr debris and tracing these to their furthest extents, the debris has been found to deviate significantly from the Law & Majewski (2010) model (Belokurov et al. 2014; Koposov et al. 2015). In any case, PM measurements have enormous potential to better restrict both the progenitor orbit and the MW’s gravitational potential (e.g., Koposov et al. 2010; Carlin et al. 2012).

The astrometric capabilities available with the *Hubble*

tsohn@jhu.edu

¹ Department of Physics and Astronomy, The Johns Hopkins University, Baltimore, MD 21218, USA

² Space Telescope Science Institute, 3700 San Martin Drive, Baltimore, MD 21218, USA

³ Department of Astronomy, University of Virginia, Charlottesville, VA 22904-4325, USA

⁴ Steward Observatory, University of Arizona, 933 North Cherry Avenue, Tucson, AZ 85721, USA

⁵ LSST, 933 North Cherry Avenue, Tucson, AZ 85721, USA

⁶ Department of Astronomy, Pennsylvania State University, 525 Davey Laboratory, University Park, PA 16802, USA

Space Telescope (HST) are an order of magnitude better than what can be achieved from the ground, so *HST* has the potential to become a workhorse for measuring PMs along stellar streams in the MW halo. We have in fact demonstrated this to be the case in our Sgr Stream study of Sohn et al. (2015). While the low surface brightness of tidal streams, combined with the relatively small size of the *HST* field of view, limited the detected number of Sgr stream stars to about a few dozen stars per field, the accurate PMs allowed a confident separation of stream stars from foreground (disk) stars. This enabled an accurate measurement of the average PM of the stream. Furthermore, the accurate PMs for individual stars also allowed us to identify multiple kinematical components within the same *HST* fields. These discriminatory capabilities of *HST* are crucial when constraining properties of the MW dark halo because PM measurements of streams affected by contamination from other kinematical components can lead to erroneous interpretations. In this study, we once again rely on the *HST* to measure PMs of tidal stream stars, in this case those along the Orphan Stream.

The Orphan stream (Grillmair & Dionatos 2006b; Belokurov et al. 2006), ~ 60 deg long and only ~ 2 deg (~ 0.7 kpc) wide, is approximately five times narrower than the Sgr Stream while slightly closer to us, although a factor of ~ 2 lower in surface brightness. Given its atypical properties, the Orphan stream provides us with the opportunity to study the fainter end of the family of objects that built up the stellar halo of the MW. Belokurov et al. (2007) found a distance gradient along the stream, and also published radial velocities from sparse samples of SDSS data in two fields, one at the close end of the stream (at ~ 20 kpc) and one at the distant end of the stream (at ~ 32 kpc). Later, Newberg et al. (2010) published radial velocities for blue horizontal-branch (BHB) stars along the stream from SDSS/SEGUE, and Casey et al. (2013) and Casey et al. (2014) published K-giant spectra from AAT/AAOMEGA as well as high-resolution Magellan/IMACS follow up on their candidates. These latter studies find a significant metallicity dispersion and $[\alpha/\text{Fe}]$ trends, which support the theory that the progenitor is a dwarf spheroidal satellite. Fellhauer et al. (2007) constructed tidal disruption models assuming that the UMa II dSph is the progenitor of the stream, and concluding that some young halo globular clusters and the Complex A gas cloud may also be associated. However, this study had trouble fitting the near-field velocity data. Jin & Lynden-Bell (2007) explored in more detail the possibility that Complex A and the Orphan stream were related to each other, but they were unable to obtain a good fit under this assumption. Sales et al. (2008) and Newberg et al. (2010) both fitted orbits to the available data, and found that the orbit of the Orphan stream does not intersect either UMa II or Complex A. The data are consistent with a single wrap of the trailing arm of a fully disrupted satellite, or with a progenitor outside of the SDSS coverage area. More recently, Grillmair et al. (2015) detected the Orphan stream in the southern sky using Dark Energy Camera (DECam) observations extending the total known length of the Orphan stream to 108° . They have also found an overdensity in the stream that seems consistent with the Orphan progenitor. This finding combined with the dynamical model of Newberg et al. (2010) implies that the original detection of the stream is the leading arm.

In this paper, we present results from our *HST* project to measure PMs of individual stars along the Orphan stream. The paper is organized as follows. In Section 2, we describe

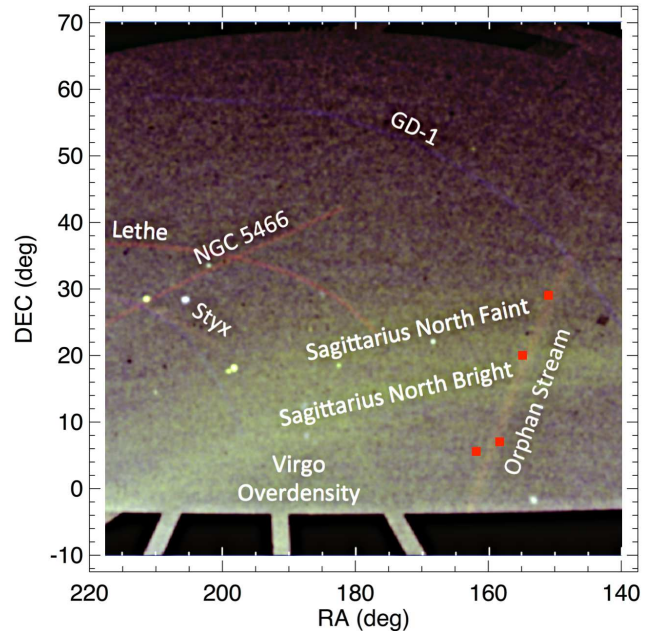


Figure 1. Partial view of the SDSS footprint showing stellar streams at various distances in equatorial coordinates (original figure from Grillmair & Carlin 2016). The two bright branches that run roughly horizontal in this figure are the Sgr Stream: the bottom one is the main stream, and the top one is known as the “faint arm.” The thin branch that runs roughly perpendicular to the Sgr Stream is the Orphan Stream. Our four *HST* target fields are overplotted as red squares. From top to bottom, these fields are denoted *ORPH-F1*, *ORPH-F2*, *ORPH-F3*, and *ORPH-F4*.

the data used for this study, and the determination of photometric and PM measurements for individual stars in our target fields. In Section 3, we describe the identification of Orphan stream stars in each of the fields based on the combined color-magnitude diagram (CMD) and PM information. We also discuss the detection of stars that possibly belong to other known stellar streams (e.g., the Sgr Stream). In Section 4, we explore the 2-d motions of stars on the sky based on our PM measurements, and discuss the nature of the known and newly discovered kinematical components. Finally, we summarize our results in Section 5.

2. OBSERVATIONS AND DATA ANALYSIS

2.1. First- and Second-epoch Data

The original goal of this project was to measure *HST* PMs of stars located along the Orphan stream using *HST* data. To achieve this goal, we searched the *HST* archive for existing deep imaging serendipitously located in the vicinity of the Orphan stream. We identified and selected four fields (Figure 1) with characteristics as summarized in Table 1. We note that fields *ORPH-F1* and *-F2* are located close to the densest parts of the stream ($B_{\text{Orphan}} \lesssim 0.3$ deg, where B_{Orphan} refers to the orthogonal distance to the Orphan Stream as defined by Newberg et al. 2010), whereas the other two fields (*ORPH-F3* and *-F4*) are offset from the center of the stream by more than 1 deg in their closest points on the sky. Interestingly, two of our target fields happen to be also located on the two separated arms of the Sgr Stream: *ORPH-F1* is on the faint arm (or branch B as denoted by Belokurov et al. 2006) and *ORPH-F2* is on the bright arm (or branch A).

The first-epoch data of our target fields were observed for various *HST* programs (see Table 1). The second-epoch data were obtained through our *HST* Program GO-13443 (PI: R.

van der Marel). We targeted the four fields using the same observational setups (i.e., pointing, telescope orientation, detector, and filters) as the first-epoch observations. For astrometry, we observed with the ACS/WFC detector using F814W for *ORPH-F1* and *-F4*, and F775W for *ORPH-F2* and *-F3* to match the first-epoch data. Hereafter, we denote both of these filters as *I*-band unless there is a need to make a distinction between them. During our second-epoch observations, we also obtained F606W exposures to obtain color information of stars in our target fields for constructing CMDs.

2.2. PM Measurements and Photometry

PMs of stars in our target fields were measured using the same technique as we used in Sohn et al. (2015) for measuring PMs of stars along the Sgr Stream. In summary, we stacked high-resolution images using our deeper second-epoch observations, identified stars and background galaxies from the stacks, created background galaxy templates, measured positions of stars and galaxies on images in each epoch with the templates, and measured shifts in positions of stars with respect to the background galaxies between the two epochs. In addition to the PMs, we have also measured photometry for each star in our target fields. For this, we combined images for each field per filter using *astrodrizzle*, measured stars within aperture radii of 0.1 mas (4 ACS/WFC pixels), and carried out aperture corrections to infinity following the method provided by Sirianni et al. (2005). We then calibrated the photometry to the ACS/WFC VEGAMAG system using the time-dependent zero points provided by the STScI webpage.⁷

3. IDENTIFICATION OF STARS IN THE ORPHAN STREAM

Our target fields are expected to contain not only stars that belong to the Orphan stream, but also other stars in the foreground or background. We follow a similar method used in Sohn et al. (2015) for identifying stars associated with the Orphan stream using the information provided by the CMDs and PM diagrams. Specifically, we first overlay fiducial isochrones developed by the Dartmouth Stellar Evolution Database (Dotter et al. 2008) on the CMDs that represent the Orphan stream stellar population, and select stars consistent with these isochrones. The stars in the Orphan stream are known to be mainly old and metal-poor with metallicities ranging from $[\text{Fe}/\text{H}] = -1.5$ to -2.5 according to spectroscopic observations (Newberg et al. 2010; Sesar et al. 2013; Casey et al. 2013). Therefore, we decided to overlay isochrones with an age of 12 Gyr and with three different metallicities ($[\text{Fe}/\text{H}] = -1.5, -2.0,$ and -2.5) that encompass the spectroscopic metallicity range of most stars identified as Orphan stream stars in previous spectroscopic surveys.⁸ For the distance to the Orphan stream at each field location, we adopted the heliocentric distance based on the orbital model by Newberg et al. (2010). Their models were tailored to fit the observed that of BHB stars along the Orphan stream and, because Sesar et al. (2013) finds that Newberg et al. (2010)'s Model 5 fits the distance of RRab stars fairly well, that was our model of choice. Finally, we applied reddening to the isochrones based on the $E(B-V)$ values estimated from interpolating the reddening maps of Schlegel, Finkbeiner, & Davis

(1998). The total absorption values were then adopted from Table 6 of Schlafly & Finkbeiner (2011). We note that the foreground reddening of our target field is generally very low, with $E(B-V)$ values in the range 0.019–0.022. The isochrones are plotted in black lines in the CMD of each field. Stars are considered to be consistent with an Orphan-like population if they lie on one of the isochrones (or in between two of the isochrones) within their color errors. We note that the exact choice for the stream's stellar population properties, reddening, or distance are not critical for this study as our main purpose is to determine which stars in each observed CMD are reasonably associated with the Orphan stream.

Once candidate member stars are selected based on their location in the CMDs, we inspect the PM diagrams to locate tight clumps that represent kinematically-cold groups of stars. If such clumps exist, they are compared to the PM predictions provided by Newberg et al. (2010) to check whether they are consistent with belonging to the Orphan stream.⁹ The Newberg et al. (2010) model was tailored to fit the observed positions, distances, and line-of-sight velocities of Orphan stream stars under a realistic MW potential, and therefore the PMs predicted by this model are expected to provide a reasonable first order guess of the true PMs.

In addition to the stars of interest, our target fields will also contain MW stars in the foreground and background. It is therefore important to assess the number of MW stars in our PM diagrams. Foreground stars in the MW disk are in general not a concern since most of them are typically far redder than the isochrones used for selecting old stellar populations. Moreover, their PM distribution has a large spread of several mas yr^{-1} and do not clump in PM space (see, e.g. Deason et al. 2013). Halo stars of the MW are more difficult to separate from stellar streams since they share similar properties in terms of stellar populations (and distances in some cases). Typically, there are a handful of MW halo stars predicted per field with a dispersion of order $\sim 1 \text{ mas yr}^{-1}$ as we have shown in Sohn et al. (2015). To quantitatively predict the PM distribution of MW halo stars in each of our fields, we followed the same methodology used in that study. In short, we adopted the Besançon model (Robin et al. 2003) for each field location, selected model stars that satisfy our CMD selection criteria, and estimated the number of MW halo stars in each ACS/WFC field. In each of our PM diagrams (Figures 2b, 4b, 5b, and 6b), we also show the median value and the 68% confidence interval of the PM distribution of MW halo stars as a gray cross. A general discussion of the predicted PMs of MW stars in *HST* fields is detailed in Section 3.1.3 of Sohn et al. (2015).

Finally, if we find a significant excess of stars against our estimates of both Orphan stream and MW halo stars, there is a possibility of other kinematical groups existing in our fields. In this case, we go back to the CMD to check for additional populations of stars at any given distance. For this, we use old and metal-poor isochrones because all stellar streams found in the MW halo so far are predominantly old and metal poor.

3.1. ORPH-F1

In Figure 2, we plot CMDs and PM diagrams for the *ORPH-F1* field. The expected heliocentric distance to the Orphan Stream for this field location is 34 kpc and a reddening of $E(B-V) = 0.023$ was used. The isochrones represent-

⁷ <http://www.stsci.edu/hst/acs/analysis/zeropoints>.

⁸ The choice of age for our isochrones is not important since, as will be shown, all of the stars we identify lie in the CMD fainter than the main sequence turnoff.

⁹ So far, the only existing PM models in the literature are those of Newberg et al. (2010).

Table 1
HST Target Fields and Observations

Target Fields	R.A.	Decl.	$\Lambda_{\text{Orphan}}^a$	B_{Orphan}^a	Epoch 1		Epoch 2 (Prog. ID 13443)		
	(J2000)	(J2000)	(deg)	(deg)	Prog. ID	Epoch	Exp. Time (s) ^b	Epoch	Exp. Time (s) ^b
<i>ORPH-F1</i>	10:03:48.9	+29:06:12.8	-11.96	-0.31	9468	2003.29	6000	2014.23	7339
<i>ORPH-F2</i>	10:19:16.4	+20:02:11.6	-2.23	-0.27	9575	2002.41	3100	2014.24	7284
<i>ORPH-F3</i>	10:33:12.9	+07:03:15.4	11.11	1.20	9984	2003.90	2444	2014.97	7072
<i>ORPH-F4</i>	10:47:26.8	+05:35:22.4	13.66	-1.61	9877	2004.36	3630	2014.28	7234

^a Coordinate system of the Orphan stream as defined by Newberg et al. (2010).

^b Total exposure time of the *I*-band observations used for astrometric analysis.

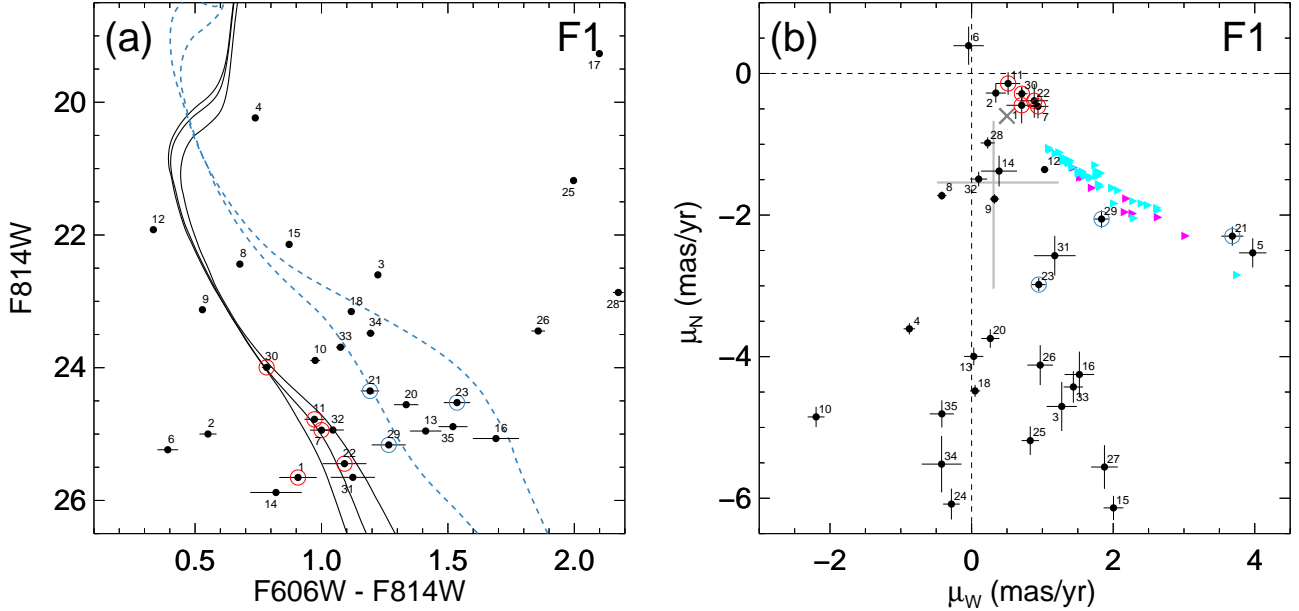


Figure 2. Selection of stars associated with stellar streams in *ORPH-F1*. Panel (a) shows the observed *I* vs. *V*–*I* CMD and panel (b) shows the observed PM diagram. The observed stars in the field are shown as black symbols in all panels, with the associated error bars shown in both panels. Numbers are provided for each star in each panel to aid cross identification. Not all stars in panel (a) are shown in panel (b) due to their PMs being outside the range of panel (b). For most stars, the *F814W* magnitude errors in panel (a) are smaller than the plot symbols. In panel (a), the black solid curves are fiducial isochrones for old (12 Gyr) populations with metallicities of $[\text{Fe}/\text{H}] = -1.5, -2.0,$ and -2.5 (from right to left) at a distance of 34 kpc. The blue dashed curves are fiducial isochrones for an old and metal-poor (11 Gyr, $[\text{Fe}/\text{H}] = -1.8$), and an intermediate-age and metal-rich (5 Gyr, $[\text{Fe}/\text{H}] = -0.5$) populations at distances of 17 kpc. The black solid curves are used for identifying the Orphan stream population, while the blue dashed curves are used for identifying potential Sgr Stream stars. Red and blue circles in both panels highlight stars that are identified as potential Orphan and Sgr Stream stars, respectively. The cross mark in panel (b) indicates the predicted PM from the orbital model by Newberg et al. (2010). In the same panel, we also show the Law & Majewski (2010) *N*-body model leading-arm particles in right-facing triangles to provide PM predictions of the Sgr faint arm at this field location assuming that both the bright and faint arms move in parallel on the sky (see text for details). These particles are color coded following Law & Majewski (2010) such that different colors represent the time at which a given debris particle became unbound from the Sgr dSph: magenta for 1.5–3 Gyr ago; and cyan for 3–5 Gyr ago. The PMs of the model particles are offset from the original position such that their distances are decreased by 3 kpc to account for the difference in distance between the Sgr bright and faint arms. The gray cross shows the 68 confidence intervals in each coordinate for MW halo star PMs drawn from Besançon models, chosen to meet our CMD selection criteria for stars on the Orphan and Sgr streams. An expectation value of 4 MW halo stars is predicted within the area spanned by the cross.

ing an Orphan-like population are plotted as black curves in Figure 2a. Among the stars consistent with these isochrones, we find five (marked in red circles) that are clustered around $(\mu_W, \mu_N) = (0.8, -0.5) \text{ mas yr}^{-1}$. These five stars are close to the PM prediction (cross symbol in Figure 2b) for this field by Newberg et al. (2010), and we identify them as being associated with the Orphan stream. We further analyze the resulting 2-d motion on the sky for these stars in Section 4.

Upon inspecting the CMD and PM diagrams and further quantitatively comparing them to the predictions by the Besançon model, we found that there is a general excess of stars. There are two ways of viewing this: an excess in the CMD or an excess in the PM diagram. First, in the color range $1.0 < (F606W - F814W) < 1.7$ and magnitude range $23 < F814W < 25.5$, the Besançon model predicts only four

stars in our field of view, but we have a count of 12 stars in that color and magnitude range in Figure 2a. Second, we also find that while the Besançon model predicts only one star in total (regardless of which MW component it belongs to) per ACS/WFC field in the PM range of $\mu_N < -3.5 \text{ mas yr}^{-1}$, our PM diagram (Figure 2b) shows 14 stars significantly in excess of model predictions for the MW disk and a smooth halo. We first discuss the excess as seen in the CMD, and then explore the excess in the PM diagram.

Our *ORPH-F1* field is located close to the “faint arm” of the Sgr Stream (see Figure 1) on the sky, so we expect to find stars from this component. So far, there is no successful model that explains the bifurcation of the Sgr Stream, but the Sgr faint arm has been mapped in both the Northern (Belokurov et al. 2006) and South-

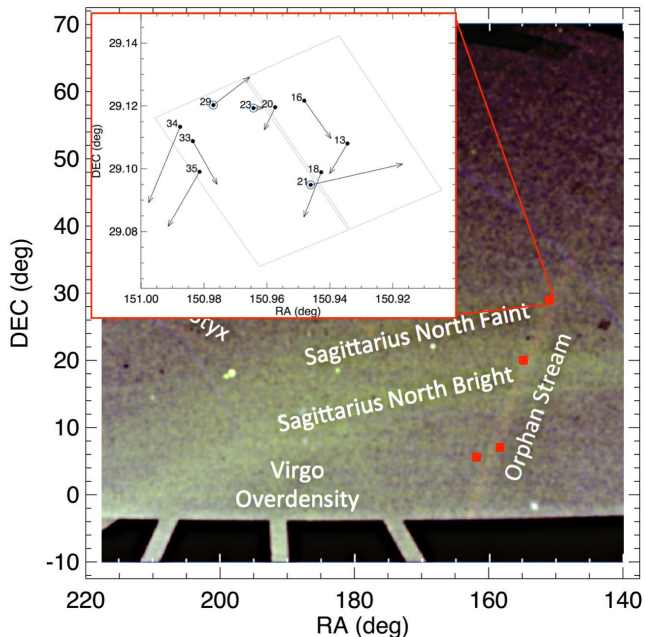


Figure 3. Same as Figure 1, but the inset now shows the 2-d motion on the sky (arrows) of individual stars selected via CMD as being consistent with a Sgr-like population at the distance of 17 kpc. The gray lines show the boundary of the ACS/WFC images on the sky, and black dots are the CMD-selected stars as discussed in the text. Each star is identified using the same number as in Figure 2. The length of each vector is scaled in a relative sense to show the difference in speed assuming that all stars are at distances of 17 kpc. The stars with blue circles are possible candidates of the Sgr faint arm based on their based on their 2-d motions.

ern hemispheres (Koposov et al. 2012; Slater et al. 2013; de Boer, Belokurov, & Koposov 2015). The faint arm has been consistently measured to be about 5 kpc closer to us than the bright arm at any given Sgr longitude (see e.g., Figure 7 of Slater et al. 2013). In the Sgr coordinates defined by Majewski et al. (2003), our *ORPH-F1* field is located at $\Lambda_{\odot} = 220^{\circ}.7$, and the heliocentric distance of the bright arm at this Sgr longitude is ~ 22 kpc based on Figure 4 of Belokurov et al. (2014). Therefore, stars on the Sgr faint arm, if present, are expected to be at a distance of ~ 17 kpc in this part of the sky. The Sgr bright arm is known to have a mixed population of stars: an old and metal-poor population + an intermediate-age metal-rich population. In our Sgr stream study (Sohn et al. 2015), we have found that stars from both of these populations are detected even in the small fields of *HST*. We therefore overlaid isochrones of (age, [Fe/H]) = (12 Gyr, -1.5) and (5 Gyr, -0.5) with distances of 17 kpc in our CMD, and first selected 10 stars that lie close to or in between these two isochrones. We then inspected the 2-d motions of these 10 stars on the sky and compared them with the Sgr faint arm to select candidate member stars.

While we currently have no existing information on the predicted PM of the Sgr faint arm, we can select stars based on the fact that any star that belongs to the Sgr faint arm should follow the direction of the overall distribution of the stream (extending from southeast to northwest on the sky) to first order. The observed PM of any star on the sky includes a contribution from the solar motion, so we need to subtract that to get the 2-d motion on the sky. For this, we assumed a distance to the Sun from the Galactic center of $R_0 = 8.29$ kpc, a circular velocity of the local standard of rest (LSR) of $V_0 = 239$ km s^{-1} (McMillan 2011), and a solar peculiar velocity with re-

spect to the LSR of $(U, V, W)_{\text{pec}} = 11.10, 12.24, 7.25$ km s^{-1} (Schönrich, Binney, & Dehnen 2010). The PM contribution of the solar motion also depends on the distance to the target object, so we used the distance of 17 kpc. At this distance, the PM contribution from the solar motion toward the *ORPH-F1* field is $(\mu_W, \mu_N) = (0.63, -2.99)$ mas yr^{-1} . This motion was *subtracted* from the observed PM of each star to obtain a net 2-d motion on the sky. The resulting 2-d vectors compared to the Sgr faint arm are shown in Figure 3. We find that the three stars circled in blue in Figure 2 (stars 21, 23, and 29) have 2-d motions consistent with the Sgr faint arm. However, we note that the PMs of these three stars are not clumped together in Figure 2b which indicates it is unlikely that all three stars are members of the Sgr faint arm. Without a detailed dynamical model that explains the Sgr faint arm, it is difficult to determine which of these three stars belong to the Sgr stream. We can however obtain a first-order guess of where the stars should be placed in the PM diagram assuming that both the bright and faint arms of the Sgr move in parallel on the sky. For this, we selected model particles from the *N*-body model of Law & Majewski (2010) that are located within 1° from the same Sgr longitude as our *ORPH-F1* field, and corrected the model PM predictions for the difference in distance (3 kpc) between the bright and faint arms. The resulting model particles are shown in Figure 2b. Based on comparing the model and observations, star 29 is most likely a star that belongs to the Sgr faint arm, while the other two stars are less likely to be so.

The excess of stars in our PM diagram for $\mu_N < -3.5$ mas yr^{-1} indicates that there may be substructures (stellar streams or kinematically-cold groups) other than the Sgr and Orphan Streams in the halo in this part of the sky at distances closer than 17 kpc. However, we have not found any obvious PM clumps in this field that correspond to the same stellar population at the same distance based on the CMD.

3.2. *ORPH-F2*

Figure 4 shows the CMD and PM diagram for the *ORPH-F2* field. For the CMD, we adopted the same fiducial isochrone as used for the *ORPH-F1* field but with a distance of 29 kpc. Unlike the case for *ORPH-F1* field, we do not find any noticeable clump in the PM diagram. There is only one star (circled in red) that is consistent with being an Orphan-like population, and close enough to the PM prediction by Newberg et al. (2010). Without further information, it is difficult to judge whether this star actually belongs to the Orphan stream or is just a random halo star. Therefore, the identification of Orphan stream stars in this field is tentative.

The *ORPH-F2* field is located on the main Sgr stream (or the bright arm) at $\Lambda_{\odot} = 226^{\circ}.4$, and we expect Sgr Stream stars to be present in this field. We have overlaid the same age+metallicity isochrones used in the *ORPH-F1* field for identifying Sgr stream stars, but at a distance of 22 kpc based on Figure 4 of Belokurov et al. (2014). Among the stars consistent with these isochrones, seven stars are easily identified as a conspicuous clump in the PM diagram. These are plotted in blue circles in Figure 4. For comparison, we also plot the Law & Majewski (2010) *N*-body model particles that are within 1.5° in both right ascension and declination from the center of our *HST* field. The observed PM clump is very close to the model particles as expected, and similar to the findings for Sgr *FIELD 4* in Sohn et al. (2015) at $\Lambda_{\odot} = 251^{\circ}.1$. Beyond these, no other significant excess has been found in the PM diagram.

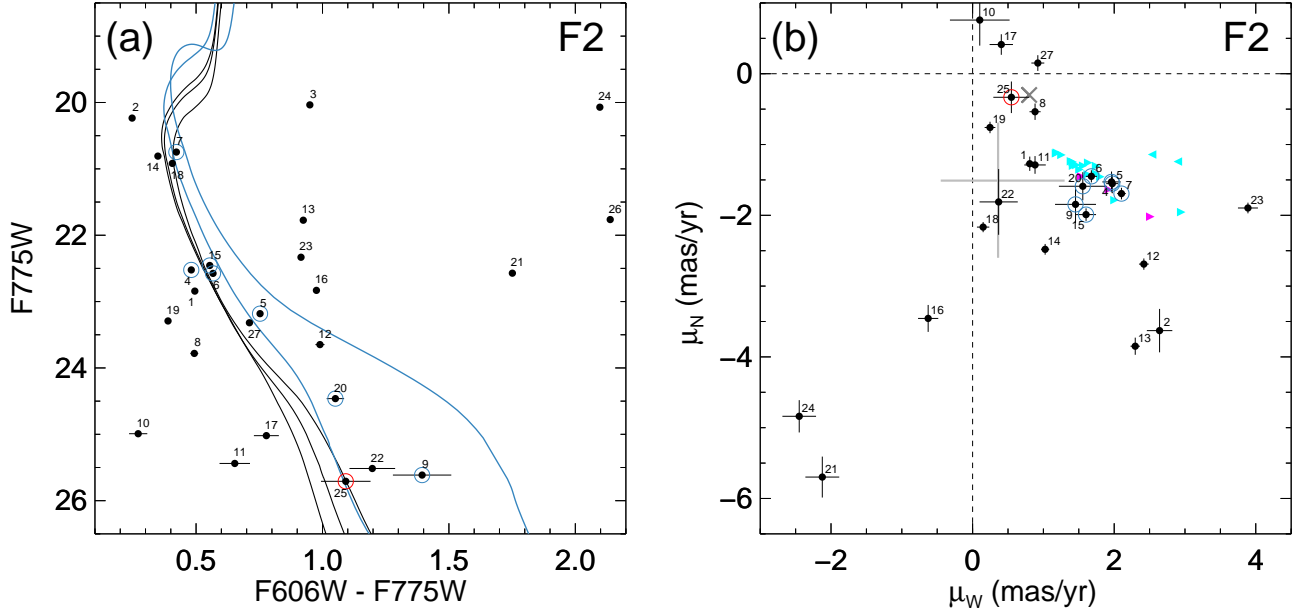


Figure 4. Selection of stars associated with stellar streams in the *ORPH-F2* field. The panels and symbols are similar to those in Figure 2. The black solid curves in panel (a) are the same isochrones as used in Figure 2 but for a distance of 29 kpc. For the Sgr Stream, solid blue lines are used in panel (a) instead of dashed blue lines to represent the Sgr bright arm, and the distance of 23 kpc was adopted for these isochrones. In panel (b), we also show the Law & Majewski (2010) N -body model particles in right- (leading) or left-facing (trailing) triangles. These particles are color coded following Law & Majewski (2010) such that different colors represent the time at which a given debris particle became unbound from the Sgr dSph: magenta for 1.5–3 Gyr ago; and cyan for 3–5 Gyr ago. The gray cross is the same as in Figure 2. An expectation value of 3 MW halo stars is predicted within the area spanned by the gray cross.

3.3. *ORPH-F3*

Figure 5 shows the CMD and PM diagram for the *ORPH-F3* field. If present, Orphan stream stars should be at a distance of 24 kpc. We used the fiducial isochrones to identify Orphan stream stars, and found four stars consistent with the isochrones within their photometric errors. However, all of these stars are far away from the PM prediction of Newberg et al. (2010). There is only one star (22) that is close enough to the model prediction to be considered a member of the Orphan stream, but its color ($F606W - F775W \simeq 0.8$) is too red for its brightness to be considered an Orphan stream star. We conclude that there is no star associated with the Orphan stream in this field. Given that this field is about 1.2° away in the orthogonal direction from the densest part of the Orphan stream, and given that the Orphan stream is a thin stellar stream, it is unsurprising to find no star in a small *HST* ACS field.

Upon inspecting the CMD and PM diagram further, we found stars that possibly belong to a kinematically cold component at the distance of ~ 32 kpc from us. The three stars, shown in green circles, are well described by an isochrone with (age, $[\text{Fe}/\text{H}]$, distance) = (12 Gyr, -2.5 , 32 kpc), and form a clump in the PM diagram at $(\mu_N, \mu_W) \approx (-0.1, -1.3)$. We discuss the nature of this clump in Section 4. We further attempted to identify other PM clumps in this field, but did not find any that seem to belong to the same stellar population based on shifting old and metal-poor isochrones in the CMD.

3.4. *ORPH-F4*

Figure 6 shows the CMD and PM diagram for the *ORPH-F4* field. This field is located almost on the opposite side of the *ORPH-F3* field with respect to the Orphan stream, and is about 1.6° away from the densest part of the Orphan stream. Therefore, the expected number of Orphan stream stars is even lower than in the case of *ORPH-F3*. The only star (#31)

close to the model prediction in the PM diagram of Figure 6b is too blue in color for its brightness to be a Orphan stream star, so we conclude that we do not detect any star that belongs to the Orphan stream in this field.

As with the *ORPH-F3* field, we searched for additional kinematically cold components, and found 3 stars that possibly belong to one at the distance of ~ 12 kpc.¹⁰ The 3 stars circled in orange in Figure 6a are well described by an isochrone with (age, $[\text{Fe}/\text{H}]$, distance) = (12 Gyr, -1.5 , 11 kpc), and form a clump in the PM diagram at $(\mu_N, \mu_W) \approx (1.0, -1.7)$. We discuss the nature of this clump in Section 4.

We also found a significant excess of stars in our PM diagram (Figure 6b) at $\mu_N < -3 \text{ mas yr}^{-1}$. Our diagram shows 15 stars, but the Besançon model predicts only two stars in total per ACS/WFC field in the same PM range. However, we were not able to further identify PM clumps that belong to the same stellar population at the same distance.

4. AVERAGE MOTIONS OF STARS IN OUR TARGET FIELDS

The analysis in Section 3 has yielded a list of stars that belong to several different kinematical components in our target fields. In Table 2, we provide a list of individual proper motions and photometry for stars identified as members of various stellar streams based on our analysis in Section 3. Using this list, we first calculated the average PM of stars in each component and its associated uncertainty. When calculating average PMs for an individual sample, we adopted the error-weighted mean, and the error was computed by propagating the individual PM uncertainties. The results are presented in Table 3. For each component, we also list an estimate of the average intrinsic one-dimensional dispersion σ transverse to

¹⁰ Note that we used the brightest star (14) among the three to estimate the distance to this kinematically cold component because that star has the smallest color and magnitude error.

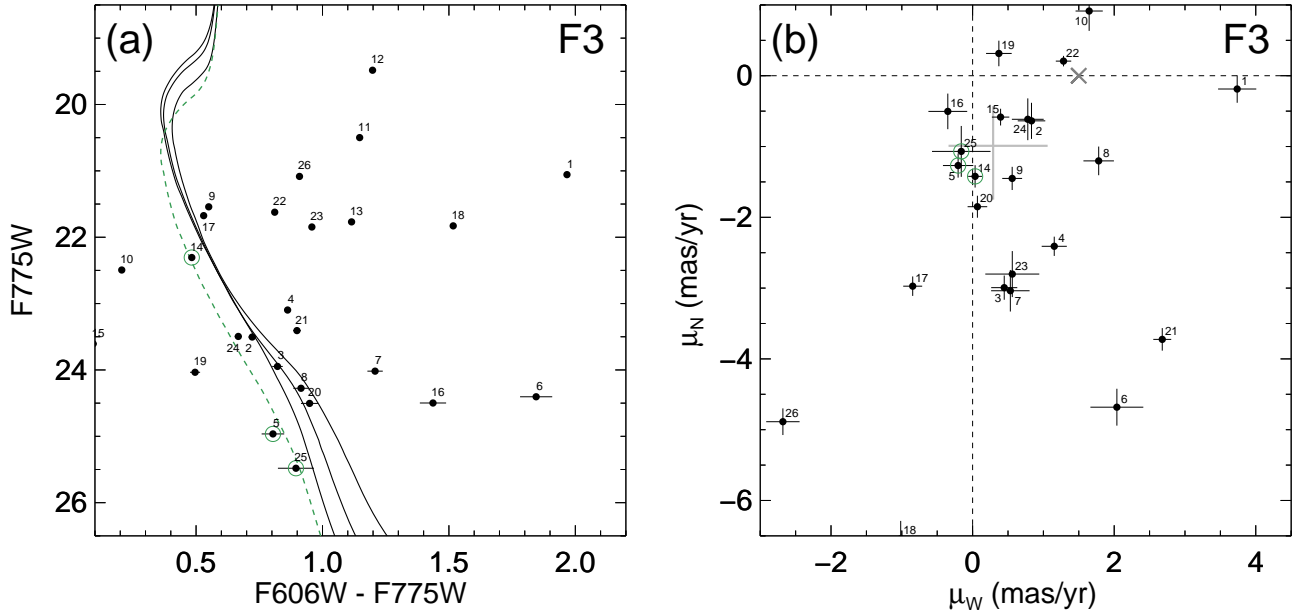


Figure 5. Selection of stars associated with stellar streams in the *ORPH-F3* field. The panels and symbols are similar to those in Figure 2. The black solid curves in panel (a) are the same isochrones as used in Figure 2 but for a distance of 24 kpc. The dashed green curve is a fiducial isochrone for a population with an age of 12 Gyr and a metallicity of $[Fe/H] = -2.5$ at a distance of 32 kpc. This isochrone is used to identify stars possibly associated with the “Parallel” stream (green circles). The gray cross is the same as in Figure 2, but for CMD selection criteria of the newly identified stream. An expectation value of 2 MW halo stars is predicted within the area spanned by the gray cross.

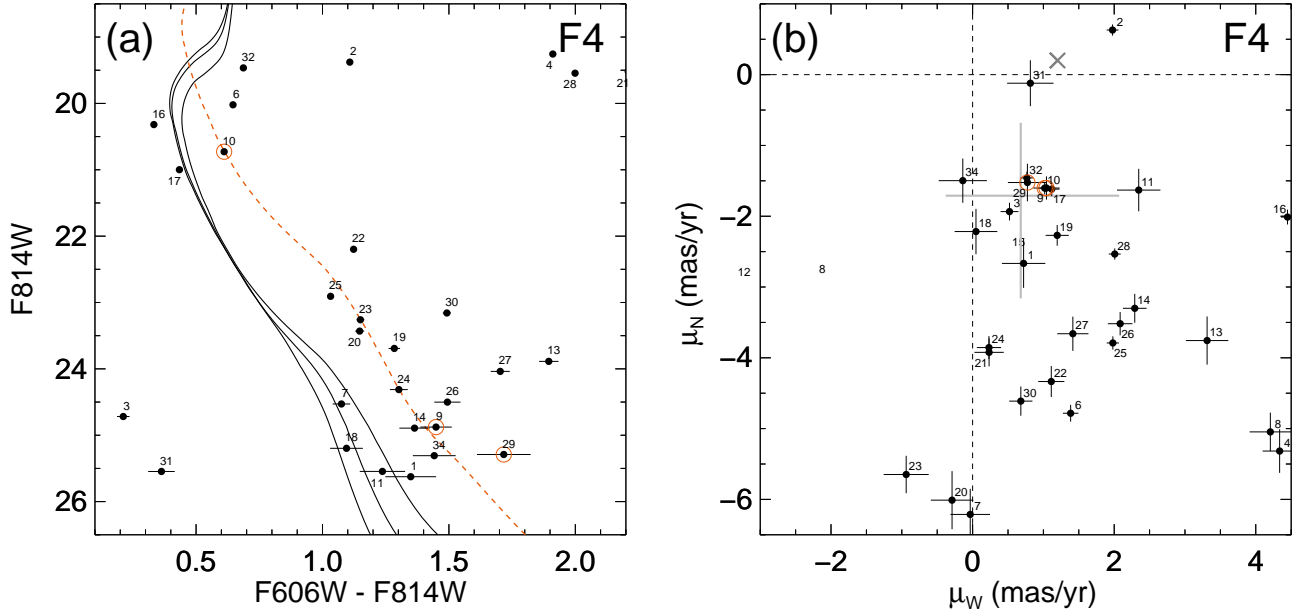


Figure 6. Selection of stars associated with stellar streams in the *ORPH-F4* field. The panels and symbols are similar to those in Figure 2. The black solid curves in panel (a) are the same isochrones as used in Figure 2 but for a distance of 23 kpc. The dashed orange curve is a fiducial isochrone for a population with an age of 12 Gyr and a metallicity of $[Fe/H] = -1.5$ at a distance of 12 kpc. This isochrone is used to identify stars possibly associated with the Lethe Stream (orange circles). The gray cross is the same as in Figure 2, but for CMD selection criteria of the Lethe Stream. An expectation value of 4 MW halo stars is predicted within the area spanned by the gray cross.

the line-of-sight in both mas yr^{-1} and kms^{-1} .
 Using the average PM of each kinematical component, we can describe their 2-d motions on the sky. This allows us to visually confirm whether our measured PM is consistent with the directions of the spatial extents of the Orphan and Sgr Streams, or to associate the newly found kinematical components to other known streams. The observed PM of any star on the sky includes a contribution from the solar motion, so we need to subtract that to get the 2-d motion on the sky as we

have demonstrated for individual stars in Section 3.1. The PM contribution of the solar motion also depends on the distance to the target object, so we used the distance to each kinematical component as estimated in Section 3.

4.1. *Orphan and Sagittarius Stream Stars*

The Orphan stream stars we found in the *ORPH-F1* field are at a distance of ~ 34 kpc, and the PM contribution from the solar motion at this distance is $(\mu_W, \mu_N) =$

Table 2
Proper motions and photometry of stars identified as stream members in each field

No.	R.A. (J2000.0) (hh:mm:ss.sss)	Decl. (J2000.0) (dd:mm:ss.ss)	μ_W (mas yr ⁻¹)	μ_N (mas yr ⁻¹)	F814W or F775W ^a (VEGAMAG)	F606W (VEGAMAG)	Stream
<i>ORPH-F1</i>							
1	10:03:37.786	+29:05:45.97	0.71 ± 0.22	-0.45 ± 0.26	25.65 ± 0.03	26.56 ± 0.07	Orphan
7	10:03:46.959	+29:08:12.53	0.94 ± 0.15	-0.46 ± 0.17	24.94 ± 0.02	25.94 ± 0.04	Orphan
11	10:03:43.184	+29:06:07.52	0.52 ± 0.17	-0.14 ± 0.16	24.78 ± 0.02	25.75 ± 0.04	Orphan
22	10:03:45.787	+29:05:00.63	0.88 ± 0.20	-0.39 ± 0.24	25.45 ± 0.04	26.54 ± 0.08	Orphan
30	10:03:54.727	+29:06:57.56	0.71 ± 0.08	-0.29 ± 0.09	24.00 ± 0.01	24.78 ± 0.02	Orphan
29	10:03:54.485	+29:07:12.94	1.84 ± 0.10	-2.06 ± 0.12	25.16 ± 0.02	26.43 ± 0.06	Sgr Faint?
<i>ORPH-F2</i>							
4	10:19:07.628	+20:01:17.32	1.96 ± 0.13	-1.53 ± 0.15	22.52 ± 0.01	23.00 ± 0.01	Sgr
5	10:19:08.159	+20:01:29.91	1.97 ± 0.09	-1.55 ± 0.14	23.18 ± 0.01	23.93 ± 0.01	Sgr
6	10:19:09.386	+20:02:05.84	1.68 ± 0.08	-1.45 ± 0.09	22.57 ± 0.01	23.14 ± 0.01	Sgr
7	10:19:08.624	+20:01:17.95	2.10 ± 0.06	-1.69 ± 0.08	20.75 ± 0.00	21.17 ± 0.00	Sgr
9	10:19:12.261	+20:03:44.42	1.45 ± 0.29	-1.85 ± 0.26	25.61 ± 0.04	27.01 ± 0.11	Sgr
15	10:19:12.869	+20:01:01.52	1.60 ± 0.14	-1.99 ± 0.09	22.46 ± 0.01	23.01 ± 0.01	Sgr
20	10:19:17.706	+20:01:18.79	1.56 ± 0.34	-1.59 ± 0.20	24.46 ± 0.02	25.51 ± 0.03	Sgr
25	10:19:19.969	+20:01:04.59	0.55 ± 0.26	-0.33 ± 0.22	25.71 ± 0.05	26.80 ± 0.09	Orphan?
<i>ORPH-F3</i>							
5	10:33:17.340	+07:01:29.63	-0.20 ± 0.21	-1.27 ± 0.17	24.96 ± 0.03	25.77 ± 0.04	Parallel
14	10:33:13.766	+07:02:39.48	0.04 ± 0.10	-1.42 ± 0.16	22.31 ± 0.00	22.79 ± 0.01	Parallel
25	10:33:08.859	+07:02:43.71	-0.16 ± 0.41	-1.07 ± 0.36	25.48 ± 0.04	26.38 ± 0.06	Parallel
<i>ORPH-F4</i>							
9	10:47:22.903	+05:37:31.78	1.04 ± 0.19	-1.60 ± 0.16	24.88 ± 0.02	26.33 ± 0.06	Lethe
10	10:47:19.105	+05:35:57.16	1.02 ± 0.10	-1.60 ± 0.09	20.73 ± 0.00	21.34 ± 0.00	Lethe
29	10:47:25.481	+05:34:21.22	0.77 ± 0.28	-1.52 ± 0.27	25.29 ± 0.03	27.01 ± 0.10	Lethe

^a F814W for fields *ORPH-F1* and *ORPH-F4*, and F775W for fields *ORPH-F2* and *ORPH-F3*

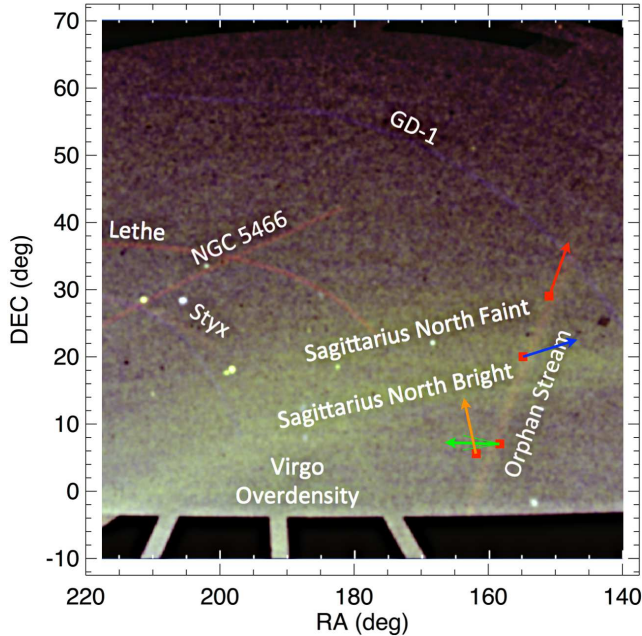


Figure 7. Same as Figure 1, but the directions of 2-d motions of stars that (possibly) belong to different streams are shown in colored arrows. Red and blue arrows are for the Orphan and Sgr Streams, respectively. Green and orange arrows are for the kinematical components found in fields *ORPH-F3* (the Parallel stream, a possible new stream) and *-F4* (the Lethe stream), respectively. The magnitude of each vector was arbitrarily chosen to show the direction of motion clearly, and does not represent the actual space velocity of each component. The thin lines next to the green arrow for field *ORPH-F3* represent the 1σ error of the 2-d motions based on the PM uncertainties. For the other fields, similar 1σ -error lines overlap with the arrows due to their small PM errors.

Table 3
Proper motion averages and dispersions

Sample	μ_W (mas yr ⁻¹)	μ_N (mas yr ⁻¹)	N_* ^a	$\frac{\sigma_{1-d}^b}{(\text{mas yr}^{-1})}$	(km s ⁻¹)
<i>ORPH-F1</i>					
Orphan	0.74 ± 0.06	-0.31 ± 0.05	5	0.14	23.0
<i>ORPH-F2</i>					
Orphan ^c	0.55 ± 0.26	-0.33 ± 0.22	1
Sgr	1.91 ± 0.10	-1.67 ± 0.09	7	0.17	16.4
<i>ORPH-F3</i>					
Parallel	-0.01 ± 0.09	-1.32 ± 0.08	3	0.14	20.9
<i>ORPH-F4</i>					
Lethe	1.00 ± 0.05	-1.60 ± 0.02	3	0.10	5.6

^a Number of stream stars included in the PM calculations.

^b Average one-dimensional velocity dispersion, obtained from the combined West and North measurements, corrected for observational scatter by subtracting the median random PM error bar in quadrature. The transformations from mas yr⁻¹ to km s⁻¹ are based on the same distances as used for the isochrones in Figures 2a–6a.

^c Tentative detection of a single star.

(0.31, -1.50) mas yr⁻¹. Therefore, the net 2-d motion of Orphan stream stars becomes $(\mu_W, \mu_N) = (0.43, 1.19)$ mas yr⁻¹. The resulting vector of motion is illustrated in Figure 7 as the red arrow. The direction of motion is well aligned with the Orphan Stream, and the Orphan stream stars found in the *ORPH-F1* field are consistent with being in the leading arm of the stream in view of the discovery of the Orphan progenitor in the southern sky (Grillmair et al. 2015).

The Sgr Stream stars found in the *ORPH-F2* field are estimated to be at a distance of ~ 23 kpc, and the PM contribution from the solar motion at this distance is $(\mu_W, \mu_N) = (0.56, -2.10)$ mas yr $^{-1}$. The net 2-d motion of the Sgr stream stars then becomes $(\mu_W, \mu_N) = (1.35, 0.43)$ mas yr $^{-1}$, and this vector of motion is illustrated in Figure 7 as the blue arrow. As with the Orphan stream case, the direction of motion is reasonably well aligned with the Sgr bright arm, and is consistent with motion along the leading arm.

4.2. Field *ORPH-F3*: Possible Association with a Newly Identified Stellar Stream

In the *ORPH-F3* field, we found three stars at the distance of ~ 32 kpc that likely belong to a group of stars moving along the same direction, given the tight clustering found in the PM diagram. To test the possibility of these three stars belonging to any known stellar stream, we first explore the 2-d motion on the sky. The PM contribution from the solar motion toward the *ORPH-F3* field at the distance of 32 kpc is $(\mu_W, \mu_N) = (0.47, -1.34)$ mas yr $^{-1}$, so the resulting net 2-d motion of the three stars becomes $(\mu_W, \mu_N) = (-0.48, 0.02)$ mas yr $^{-1}$. This implies a motion almost entirely to the east on the sky with only a slight motion toward the north. This vector of motion is illustrated in Figure 7 as the green arrow. We find that these three stars have no obvious association with any of the known streams in this figure. However, a closer inspection reveals that there is a hint of a horizontal structure that roughly runs at $\text{DEC} \simeq 6^\circ$. This may be a stellar stream undiscovered so far due to the Sgr Stream being too bright in this part of the sky. We note that this may also be an artifact created during the image processing stage. A deeper imaging survey in this region of the sky such as the Pan-STARRS or LSST may be able to reveal whether this structure is an actual stellar stream or not. For now, we tentatively call this the “Parallel stream,” since it runs parallel to the Celestial Equator. If this is a stellar stream, its progenitor is likely a disrupted dwarf galaxy instead of a star cluster based on the fact that the 1-d tangential velocity dispersion is 20.9 km s^{-1} (see Table 3, comparable to those of the Orphan and Sgr stream stars in this study).

4.3. Field *ORPH-F4*: Probable Association with the Lethe Stream

Three stars are found in the *ORPH-F4* field that likely belong to a group of stars moving in the same direction. The reflex solar motion at the distance of 12 kpc in this direction of the sky is found to be $(\mu_W, \mu_N) = (1.41, -3.50)$ mas yr $^{-1}$, so the resulting net 2-d motion of the three stars in this field become $(\mu_W, \mu_N) = (-0.41, 1.91)$ mas yr $^{-1}$. This vector of motion is illustrated in Figure 7 as the orange arrow. Unlike the case of the three stars in the *ORPH-F3* field, it is immediately apparent that the three stars in this field likely belong to the Lethe stream, another stellar stream discovered by Grillmair (2009). The Lethe stream is found to show a distance gradient decreasing from east to west: within the SDSS northern footprint used by Grillmair (2009), the distance at the eastern end is 13.4 kpc and at the western end near the Sgr stream, the distance decreases to 12.2 kpc. Our distance of 12 kpc is therefore consistent with the distance gradient found by Grillmair (2009) for the Lethe stream. The three stars we found in this field also share the same stellar population properties (metallicity and age) as the Lethe stream as found by Grillmair (2009). Finally, Grillmair (2009) concluded that Lethe is the debris stream of a globular cluster, and our mea-

sured 1-d tangential velocity dispersion of 5.6 km s^{-1} is consistent with this. We therefore conclude that the 3 stars belong to the Lethe stream.

5. SUMMARY AND CONCLUSIONS

We present high precision PMs of stars identified in four fields selected along the Orphan Stream using *HST*. The combination of PM data and photometry has allowed for unique association of groups of stars with similar ages, spatial location, and kinematics. In the *ORPH-F1* field, we identified five stars that likely belong to the Orphan stream based on their stellar population, distance, and PM information. The average PM generally agrees with the model prediction by Newberg et al. (2010). In the *ORPH-F2* field, we have a tentative detection of one star that belong to the Orphan stream. In the remaining two fields, we were not able to identify stars that belong to the Orphan stream.

We also serendipitously identified and measured PMs of stars that belong to two known and one unknown stellar streams. In the *ORPH-F1* field, we detected three potential candidate stars that may belong to the Sgr faint arm based on their stellar population and 2-d motions on the sky. However, our comparison to *N*-body models of Law & Majewski (2010) shows that only one of the three stars has the correct PM for being a member of the Sgr Stream. In the *ORPH-F2* field, we measured the PMs of seven stars that belong to the leading arm of the Sgr Stream. The average measured PM is consistent with the Law & Majewski (2010) model, just as we found in our Sgr Stream study (Sohn et al. 2015). In the *ORPH-F3* field, we identified three stars that likely belong to a new stream at the distance of ~ 32 kpc, which we tentatively named the Parallel Stream. The stellar population and 1-d tangential velocity dispersion suggest that the progenitor is a dwarf galaxy. Finally, in the *ORPH-F4* field, we measured for the first time the PMs of 3 stars that belong to the Lethe stream (Grillmair 2009). The distance, stellar populations, net 2-d motion on the sky, and 1-d tangential velocity dispersion of the three stars are all consistent with the Lethe stream as their origin.

Finally, we found that fields *ORPH-F1* and *ORPH-F4* show significant excess in their observed PM diagrams when compared to the Besançon model. This indicates that there are likely additional substructures in these parts of the sky, but due to our limited field of view, we were not able to identify them in our study. A deep and wide photometric or astrometric survey (e.g., *Gaia*) of these areas may reveal unknown substructures.

As part of an ongoing *HST* archival legacy program (AR-13272, PI: R. P. van der Marel) to determine PMs of metal-poor halo stars in random pointings multiply imaged by *HST*, we expect further PM measurements of stars that belong to known and unknown stellar streams.

Once its final catalog is released, the *Gaia* mission will enable mapping of the entire extent of each stellar stream as well as the discovery of new stellar streams in the Galactic halo. However, for distances beyond ~ 10 kpc, only *HST* is able to measure useful PMs for old stellar populations on a star-by-star basis. This study has illustrated the power of combining the high accuracy PMs and deep photometry allowed by *HST* to uniquely identify dynamically associated groups of stars. As such, *HST* will continue to be greatly advantageous and complementary to the *Gaia* mission in this research area.

We thank the anonymous referee for constructive feedback that helped improve the presentation of our results. Support for this work was provided by NASA through a grant for program GO-13443 from the Space Telescope Science Institute (STScI), which is operated by the Association of Universities for Research in Astronomy (AURA), Inc., under NASA contract NAS5-26555. SRM acknowledges support from grant nsf-ast1312863.

Facilities: HST(ACS/WFC).

REFERENCES

- Belokurov, V., Zucker, D. B., Evans, N. W., et al. 2006, *ApJL*, 642, 137
 Belokurov, V., Evans, N. W., Irwin, M. J., et al. 2007, *ApJL*, 658, 337
 Belokurov, V., Koposov, S. E., Evans, N. W., et al. 2014, *MNRAS*, 437, 116
 Bovy, J. 2016, *Phys. Rev. Lett.*, 116, 121301
 Carlberg, R. G. 2012, *ApJ*, 748, 20
 Carlberg, R. G., Grillmair, C. J., & Hetherington, N. 2012, *ApJ*, 760, 75
 Carlin, J. L., Majewski, S. R., Casetti-Dinescu, D. I., et al. 2012, *ApJ*, 744, 25
 Casey, A. R., Da Costa, G., Keller, S. C., & Maunder, E. 2013, *ApJ*, 764, 39
 Casey, A. R., Keller, S. C., Da Costa, G., Frebel, A., & Maunder, E. 2014, *ApJ*, 784, 19
 Debattista V. P., Roškar, R., Valluri, M., et al. 2013, *MNRAS*, 434, 2971
 de Boer, T. J. L., Belokurov, V., & Koposov, S. 2015, *MNRAS*, 451, 3489
 Deason, A. J., van der Marel, R. P., Guhathakurta, P., Sohn, S. T., & Brown, T. M. 2013, *ApJ*, 766, 24
 Deg, N., & Widrow, L. 2013, *MNRAS*, 428, 912
 Dotter, A., Chaboyer, B., Jevremović, D., et al. 2008, *ApJS*, 178, 89
 Erkal, D., & Belokurov, V. 2015a, *MNRAS*, 450, 1136
 Erkal, D., & Belokurov, V. 2015b, *MNRAS*, 454, 3542
 Fellhauer, M., Evans, N. W., Belokurov, V., et al. 2007, *MNRAS*, 375, 1171
 Grillmair, C. J. 2006a, *ApJ*, 651, L29
 Grillmair, C. J., & Dionatos, O. 2006b, *ApJ*, 643, L17
 Grillmair, C. J. 2009, *ApJ*, 693, 1118
 Grillmair, C. J., Hetherington, L., Carlberg, R. H., & Willman, B. 2015, *ApJ*, 812, L26
 Grillmair, C. J., & Carlin, J. L. 2016, in *Tidal Streams in the Local Group and Beyond*, ed. H. J. Newberg, & J. L. Carlin (Astrophysics and Space Science Library, Vol. 420; Berlin: Springer), 87
 Jin, S., & Lynden-Bell, D. 2007, *MNRAS*, 378, L64
 Johnston, K. V., Zhao, H., Spergel, D. N., & Hernquist, L. 1999, *ApJL*, 512, 109
 Johnston, K. V., Spergel, D. N., & Haydn, C. 2002, *ApJ*, 570, 656
 Koposov, S. E., Rix, H. -W., & Hogg, D. W. 2010, *ApJ*, 712, 260
 Koposov, S. E., Belokurov, V., Evans, N. W., et al. 2012, *ApJ*, 750, 80
 Koposov, S. E., Irwin, M., Belokurov, V., et al. 2014, *ApJ*, *MNRAS*, 442, L85
 Koposov, S. E., Belokurov, V., Zucker, D. B., et al. 2015, *ApJ*, *MNRAS*, 446, 3110
 Law, D. R., Majewski, S. R., & Johnston, K. V. 2009, *ApJL*, 703, 67
 Law, D. R., & Majewski, S. R. 2010, *ApJ*, 714, 229
 Majewski, S. R., Skrutskie, M. F., Weinberg, M. D., & Ostheimer J. C. 2003, *ApJ*, 599, 1082
 McMillan, P. J. 2011, *MNRAS*, 414, 2446
 Newberg, H. J., Willett, B. A., Yanny, B., & Xu, Y. 2010, *ApJ*, 711, 32
 Peñarrubia, J., Koposov, S. E., & Walker, M. G. 2012, *ApJ*, 760, 2
 Robin, A. C., Reylé, C., Derrière, S., & Picaud, S. 2003, *A&A*, 409, 523
 Sales, L. V., Helmi, A., Starkenburg, E., et al. 2008, *MNRAS*, 389, 1391
 Schlafly, E. F., & Finkbeiner, D. P. 2011, *ApJ*, 737, 103
 Schlegel, D. J., Finkbeiner, D. P., & Davis, M. 1998, *ApJ*, 500, 525
 Schönrich, R., Binney, J., & Dehnen, W. 2010, *MNRAS*, 403, 1829
 Sesar, B., Grillmair, C. J., Cohen, J. G., et al. 2013, *ApJ*, 776, 26
 Sirianni, M., Jee, M. J., Benítez, N., et al. 2005, *PASP*, 117, 1049
 Slater, C. T., Bell, E. F., Schlafly, E. F., et al. 2013, *ApJ*, 762, 6
 Sohn, S. T., Anderson, J., & van der Marel, R. P. 2012, *ApJ*, 753, 7
 Sohn, S. T., van der Marel, R. P., Carlin, J. L., et al. 2015, *ApJ*, 803, 56
 Yoon, J. H., Johnston, K. V., & Hogg, D. W. 2011, *ApJ*, 731, 58